Fusion cross section for Ni-based reactions within the relativistic mean-field formalism

M. Bhuyan[1,*] and Raj Kumar[2,†]

[1]*Instituto Tecnológico de Aeronáutica, 12.228-900 São José dos Campos, São Paulo, Brazil*

[2]*School of Physics and Materials Science, Thapar Institute of Engineering and Technology, Patiala-147004, Punjab, India*

(Received 15 June 2018; revised manuscript received 26 September 2018; published 19 November 2018)

In this theoretical study, we establish an interrelationship between the nucleon-nucleon potential and the nuclear fusion reaction cross sections at low energies. The axially deformed self-consistent relativistic mean field with nonlinear NL3* and TM1 force parameters is used to calculate the density distributions of the projectile and target nuclei, which are further used in the double-folding approach to obtain the nucleus-nucleus interaction potentials. The Wong formula is used to estimate the fusion cross section and barrier distributions from the nucleus-nucleus optical potential for Ni-based systems, which are known for fusion hindrance phenomena. The results of the application of the so-obtained nucleus-nucleus potential for the fusion cross section from the recently developed relativistic effective *NN* interactions (R3Y) are compared with the well-known, phenomenological M3Y potential. The effect of the nucleon-nucleon interaction potential on the fusion cross section, in terms of the nuclear interaction potential, is included in the present analysis. We found relatively good results from R3Y interactions below the barrier energies as compared to the M3Y potential concerning the experimental data.

DOI: 10.1103/PhysRevC.98.054610

I. INTRODUCTION

Efforts have been devoted to determining the nature of nucleon-nucleon interaction since 1932 with the discovery of the neutron by Chadwick as the heart of the nucleus in nuclear physics [1–3]. In the simplest expression, the nucleon-nucleon (*NN*) interaction is considered as central and to have a typical square-well, Gaussian, or Yukawa potentials of various ranges and strengths, which can obtain the observed phase shifts in elastic-scattering processes [1,4,5]. The traditional goal of nuclear physics is to understand the properties of atomic nuclei regarding the bare interaction between a pair of nucleons. Though substantial progress has taken place to explain it in some theoretical and experimental attempts, it remains an open problem at present. A large number of interactions have been constructed via studying *NN* scattering, but there exist extensive modifications in the scattering behavior due to the presence of the surrounding nucleons in a nucleus [4,6–9]. Further, the reconstruction of the *NN* potential through particle exchanges is made possible by the development of quantum field theory [10–13]. An effective phenomenological interaction has an appropriate form to study the nuclear structure and dynamics, which typically depend on the local density of the nucleus.

At low energy, one can assume that the interaction potential between a pair of nucleons is instantaneous and therefore the concept of a substantial theory of nuclear forces is applicable to nuclear structure calculations [14–17]. The analytical derivation of potential through particle exchange is important to understand the nuclear force as well as structural properties via the nucleus-nucleus optical potential for the study of many nuclear aspects such as nuclear radioactivity, nuclear scattering, nuclear fission, and fusion processes [18–20]. A more fundamental approach to *NN* interactions at low energies has been formulated in Refs. [11,14,17,21,22] in terms of an effective theory for nonrelativistic nucleons. It involves a few basic coupling constants, which have been determined from nucleon scattering data at low energies. Furthermore, the new effective *NN* interaction entitled the R3Y potential [18–20], which is analogous to the M3Y form [3], can be derived from the relativistic mean-field Lagrangian. This interaction depends on the relativistic force parameters and the coupling constant among the interacting mesons and their masses [18–20].

One can consider any relativistic mean-field interactions based on effective-field theoretical Lagrangian density: relativistic mean-field models with linear and/or nonlinear meson couplings (all models with names starting with L, NL, or PK, plus the models FSUGold, G1, G2, and TM1), density-dependent meson-exchange couplings (DD-ME and RHF-PK models), and zero-range point-coupling models (DD-PC1, PC-PK1, and PC-PF1 models) to generate relativistic *NN*-interaction potentials numerically for the respective force parameters. The analytical derivation of the *NN* potential can only be possible for the force parameters that contain linear and/or nonlinear self-interactions. In other words, in the case of nonlinear cross-coupling parameters (FSUGold, G1, and G2), it is not possible to obtain the analytical expression for the *NN* interaction. Hence one has to follow the numerical solution to estimate the potential [18,23–26]. See Ref. [27] for details of various relativistic force parameters and their interactions based on the abovementioned patterns of couplings. Furthermore, more details of various *NN* potentials and their applications in future studies and some

*bhuyan@ita.br

†rajkumar@thapar.edu

general and up-to-date reviews on the subject can be found in Refs. [11–13,18–21,26]. Moreover, the nucleus-nucleus optical potential is quite important for the elastic scattering of light- and heavy-ion studies, in particular for the simple one-dimensional barrier penetration model of fusion reaction and for the barrier energy, radius, and curvature via the nuclear potential and the Coulomb potential [28–30]. A microscopic description is required for calculating the interaction potential that incorporates the physical process, which can significantly influence the fusion process. The double-folding model is a widely used method to obtain the nuclear potential by integrating an *NN* interaction over the matter distributions of two colliding nuclei [28–30]. It produces the nucleus-nucleus optical potential for further use in various studies including studies of radioactive decay [18–20,31–33].

At low energy, either the system can fuse by penetrating the interaction barrier or it must have sufficient energy to overcome the Coulomb barrier to get absorb. In the present study, we have considered the Ni-based reactions, i.e., ^{58}Ni + ^{58}Ni, ^{58}Ni + ^{124}Sn, ^{58}Ni + ^{132}Sn, ^{64}Ni + ^{64}Ni, ^{64}Ni + ^{124}Sn, and ^{64}Ni + ^{132}Sn, because their fusion excitation functions are available experimentally and are also known for fusion hindrance [34–43]. Below the Coulomb barrier, the nuclear structure effects dominate the resulting fusion dynamics, whereas the centrifugal potential suppresses the structure effects at above-barrier energies. The estimation of fusion characteristics of heavy ions at extreme subbarrier energies is of great interest for understanding the reaction mechanisms in astrophysics and the synthesis of the superheavy nuclei [44–46]. Hence, it is of great interest at present to evaluate the performance of the relativistic R3Y potential along with the microscopic mean-field density to estimate the nuclear interaction potential for the study of fusion reaction at low energies. Here, most of the computational efforts are devoted to solving the Dirac equation and calculating various densities. The present calculations are limited to the spherical coordinate system to generate the nucleus-nucleus interaction potential. One may consider the coupling between fusion and other degrees of freedom to generate a multidimensional potential barrier, which enhances the fusion probabilities [44–49]. More detailed studies of the multidimensional fusion barrier and its effect on the fusion dynamics can be found in Refs. [34–48,48–56].

This paper is organized as follows. In Sec. II, we discuss the theoretical model for the relativistic mean-field approach along with the double-folding procedure to obtain microscopic nucleus-nucleus optical potentials. The use of the Wong formula to study fusion characteristics is also discussed in this section. Section III is assigned to the discussion of the results obtained from our calculations and of the possible correlations among the *NN* potentials and the fusion cross sections. Finally, a summary and a brief conclusion are given in Sec. IV.

II. RELATIVISTIC MEAN-FIELD FORMALISM

At present, quantum chromodynamics is not conceivable to describe the complete picture of the hadronic matter due to its nonperturbative properties. Hence, one needs to apply the perspective of effective field theory at low energy, known as quantum hadrodynamics (QHD) [23,24,57]. The mean-field treatment of QHD has been used widely to describe the nuclear structure and infinite nuclear matter characteristics [23–25,57–64]. In the relativistic mean-field approach, the nucleus is considered as a composite system of nucleons interacting through the exchange of mesons and photons [57,65–69]. Here, most of the computational effort is devoted to solving the Dirac equation and to calculating various densities. We have used the microscopic self-consistent relativistic mean-field (RMF) theory as a standard tool to investigate fusion study via the Wong formula. Thefollowing is a typical relativistic Lagrangian density for a nucleon-meson many-body system [23,57,59–75]:

$$\begin{aligned}\mathcal{L} = {} & \overline{\psi}\{i\gamma^{\mu}\partial_{\mu} - M\}\psi + \frac{1}{2}\partial^{\mu}\sigma\partial_{\mu}\sigma - \frac{1}{2}m_{\sigma}^{2}\sigma^{2} \\ & - \frac{1}{3}g_{2}\sigma^{3} - \frac{1}{4}g_{3}\sigma^{4} - g_{s}\overline{\psi}\psi\sigma - \frac{1}{4}\Omega^{\mu\nu}\Omega_{\mu\nu} \\ & + \frac{1}{2}m_{\omega}^{2}\omega^{\mu}\omega_{\mu} + \frac{1}{4}\xi_{3}(\omega_{\mu}\omega^{\mu})^{2} - g_{\omega}\overline{\psi}\gamma^{\mu}\psi\omega_{\mu} \\ & - \frac{1}{4}\vec{B}^{\mu\nu}\cdot\vec{B}_{\mu\nu} + \frac{1}{2}m_{\rho}^{2}\vec{\rho}^{\mu}\cdot\vec{\rho}_{\mu} - g_{\rho}\overline{\psi}\gamma^{\mu}\vec{\tau}\psi\cdot\vec{\rho}^{\mu} \\ & - \frac{1}{4}F^{\mu\nu}F_{\mu\nu} - e\overline{\psi}\gamma^{\mu}\frac{(1-\tau_{3})}{2}\psi A_{\mu}. \end{aligned} \tag{1}$$

Here ψ denotes the Dirac spinors for the nucleons. The isospin and the third component of the iso-spin are denoted by τ and τ_3, respectively. Here g_σ, g_ω, g_ρ, and $\frac{e^2}{4\pi}$ are the coupling constants for the σ, ω, and ρ mesons and the photons, respectively. The constants g_2, g_3, and ξ_3 are for the self-interacting nonlinear σ- and ω-meson fields. The masses of the σ, ω, and ρ mesons and the nucleons are m_σ, m_ω, m_ρ, and M, respectively. The quantity A_μ stands for the electromagnetic field. The vector field tensors for ω^μ, $\vec{\rho}_\mu$, and photons are given by

$$F^{\mu\nu} = \partial_{\mu}A_{\nu} - \partial_{\nu}A_{\mu}, \tag{2}$$

$$\Omega_{\mu\nu} = \partial_{\mu}\omega_{\nu} - \partial_{\nu}\omega_{\mu}, \tag{3}$$

and

$$\vec{B}^{\mu\nu} = \partial_{\mu}\vec{\rho}_{\nu} - \partial_{\nu}\vec{\rho}_{\mu}, \tag{4}$$

respectively. From the above Lagrangian density we obtain the field equations for the Dirac nucleons and the meson (i.e., σ, ω, and ρ) fields as follows:

$$\begin{aligned} & (-i\alpha\cdot\nabla + \beta(M + g_{\sigma}\sigma) + g_{\omega}\omega + g_{\rho}\tau_{3}\rho_{3})\psi = \epsilon\psi, \\ & \big(-\nabla^{2} + m_{\sigma}^{2}\big)\sigma(r) = -g_{\sigma}\rho_{s}(r) + g_{2}\sigma^{2}(r) + g_{3}\sigma^{3}(r), \\ & \big(-\nabla^{2} + m_{\omega}^{2}\big)\omega(r) = g_{\omega}\rho(r) - \xi_{3}\omega^{3}(r), \\ & \big(-\nabla^{2} + m_{\rho}^{2}\big)\rho(r) = g_{\rho}\rho_{3}(r). \end{aligned} \tag{5}$$

In the limit of one-meson exchange, for static baryonic medium, the solutions of single nucleon-nucleon potentials

for scalar (σ) and vector (ω, ρ) fields are given by

$$V_\sigma = -\frac{g_\sigma^2}{4\pi}\frac{e^{-m_\sigma r}}{r} + \frac{g_2^2}{4\pi} r e^{-2m_\sigma r} + \frac{g_3^2}{4\pi}\frac{e^{-3m_\sigma r}}{r},$$
$$V_\omega(r) = +\frac{g_\omega^2}{4\pi}\frac{e^{-m_\omega r}}{r} - \frac{\xi_3^2}{4\pi}\frac{e^{-3m_\omega r}}{r},$$
$$V_\rho(r) = +\frac{g_\rho^2}{4\pi}\frac{e^{-m_\rho r}}{r}. \quad (6)$$

As we mentioned in Sec. I, the analytical expression for the relativistic *NN* interaction is only possible for the force parameters that contain the linear and/or nonlinear self-coupling terms. In the case of relativistic forces with cross-coupling terms (i.e., FSUGold, G1, G2, etc.), one has to follow the numerical solution to generate *NN* interactions. The total effective *NN* interaction is obtained from the scalar and vector parts of the meson fields. The recently developed relativistic *NN*-interaction potential analogous to the M3Y form [3] is called the R3Y potential. Here the R3Y potential is derived for the NL3* and TM1 forces, which can predict the nuclear matter as well as the properties of the finite nuclei at very high isospin asymmetries [18–20,25,26,58,61,62,70,75–77]. The relativistic effective nucleon-nucleon interaction ($V_{\rm eff}^{\rm R3Y}$) for NL3* and TM1 forces along with the single-nucleon exchange effects is written as [3,18–20,25,26]

$$V_{\rm eff}^{\rm R3Y}(r) = \frac{g_\omega^2}{4\pi}\frac{e^{-m_\omega r}}{r} + \frac{g_\rho^2}{4\pi}\frac{e^{-m_\rho r}}{r} - \frac{g_\sigma^2}{4\pi}\frac{e^{-m_\sigma r}}{r} + \frac{g_2^2}{4\pi} r e^{-2m_\sigma r} + \frac{g_3^2}{4\pi}\frac{e^{-3m_\sigma r}}{r} - \frac{\xi_3^2}{4\pi}\frac{e^{-3m_\omega r}}{r} + J_{00}(E)\delta(r). \quad (7)$$

On the other hand, the M3Y effective interaction, obtained from a fit of the G-matrix elements based on the Reid-Elliott soft-core *NN* interaction [3], in an oscillator basis, is the sum of three Yukawa potentials (M3Y) with ranges of 0.25 fm for a medium-range attractive part, 0.4 fm for a short-range repulsive part, and 1.414 fm to ensure a long-range tail of the one-pion exchange potential (OPEP). The widely used M3Y effective interaction [$V_{\rm eff}^{\rm M3Y}(r)$] is given by

$$V_{\rm eff}^{\rm M3Y}(r) = 7999\frac{e^{-4r}}{4r} - 2134\frac{e^{-2.5r}}{2.5r} + J_{00}(E)\delta(r), \quad (8)$$

where the ranges are in fm and the strengths are in MeV. Note that Eq. (8) represents the spin- and isospin-independent parts of the central component of the effective *NN* interaction along with the OPEP contribution. Comparing Eqs. (7) and (8), we find the similarity among the behavior of the *NN* interaction, and we feel that Eq. (7) can be used to obtain the nucleus-nucleus optical potential. One can find more details in Refs. [18,19,25,26]. The nuclear interaction potential, $V_n(R)$, between the projectile (p) and the target (t) nuclei, with the respective RMF (NL3* and TM1 force parameter) calculated nuclear densities ρ_p and ρ_t, is written as

$$V_n(\vec{R}) = \int \rho_p(\vec{r}_p)\rho_t(\vec{r}_t)V_{\rm eff}(|\vec{r}_p - \vec{r}_t + \vec{R}| \equiv r)d^3r_p d^3r_t, \quad (9)$$

obtained by using the well-known double-folding procedure [3] for the M3Y potential and the recently developed R3Y interaction potential, proposed in Refs. [18,19,25,26], supplemented by a zero-range pseudopotential representing the single-nucleon exchange effects. Adding the Coulomb potential $V_C(R)$ ($=Z_pZ_te^2/R$) results in the *NN*-interaction potential $V_T(R)$ [$= V_n(R) + V_C(R)$], used for calculating the fusion properties. Because we know pairing plays an important role in nuclear bulk properties including the density distribution of open-shell nuclei, one has to consider the pairing correlation in their ground states [78]. In the case of nuclei not too far from the β-stability line, the constant-gap BCS pairing approach works reasonably well and simply to take care of the pairing correlation [79]. The present analysis includes the intermediate mass nuclei around the β stability; hence we have used the relativistic mean-field results with BCS treatment for the pairing correlation [59,61–63,70,75,80,81].

A. The Wong formula

In terms of ℓ partial waves, the fusion cross section for two nuclei colliding with the center-of-mass energy ($E_{\rm c.m.}$) is given by [82]

$$\sigma(E_{\rm c.m.}) = \frac{\pi}{k^2}\sum_{\ell=0}^{\ell_{\rm max}}(2\ell+1)P_\ell(E_{\rm c.m.}), \quad (10)$$

with $k = \sqrt{\frac{2\mu E_{\rm c.m.}}{\hbar^2}}$ and μ as the reduced mass. P_ℓ is the transmission coefficient for each ℓ, which describes the penetration of barrier $V_T^\ell(R)$, given by

$$V_T^\ell(R) = V_n(R, A_i) + V_C(R, Z_i) + \frac{\hbar^2\ell(\ell+1)}{2\mu R^2}. \quad (11)$$

Using the Hill-Wheeler [83,84] approximation, the penetrability P_ℓ, in terms of its barrier height $V_B^\ell(E_{\rm c.m.})$ and curvature $\hbar\omega_\ell(E_{\rm c.m.})$, is

$$P_\ell = \left[1 + \exp\left(\frac{2\pi\left(V_B^\ell(E_{\rm c.m.}) - E_{\rm c.m.}\right)}{\hbar\omega_\ell(E_{\rm c.m.})}\right)\right]^{-1}, \quad (12)$$

with $\hbar\omega_\ell$ evaluated at the barrier position $R = R_B^\ell$ corresponding to the barrier height V_B^ℓ, given as

$$\hbar\omega_\ell(E_{\rm c.m.}) = \hbar\left[\left|d^2V_T^\ell(R)/dR^2\right|_{R=R_B^\ell}/\mu\right]^{1/2}, \quad (13)$$

and the R_B^ℓ obtained from the condition

$$\left|dV_T^\ell(R)/dR\right|_{R=R_B^\ell} = 0.$$

Instead of solving Eq. (10) explicitly, which requires the complete ℓ-dependent potentials $V_T^\ell(R)$, Wong [82] carried out the ℓ summation in Eq. (10) *approximately* under specific conditions: (i) $\hbar\omega_\ell \approx \hbar\omega_0$, and (ii) $V_B^\ell \approx V_B^0 + \frac{\hbar^2\ell(\ell+1)}{2\mu R_B^{0\,2}}$, which means to assume $R_B^\ell \approx R_B^0$ also. In other words, both V_B^ℓ and $\hbar\omega_\ell$ are obtained for the $\ell = 0$ case. Using these approximations and replacing the ℓ summation in Eq. (10) by an integral gives, upon integration, the $\ell = 0$ barrier-based

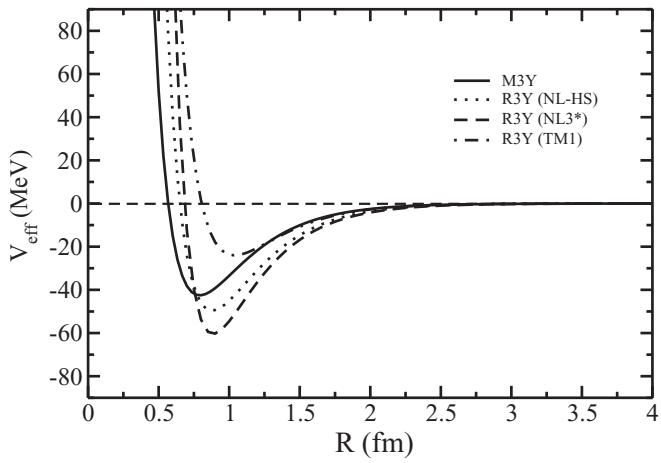

FIG. 1. The relativistic (R3Y) *NN*-interaction potential for NL-HS (linear), NL3* (nonlinear σ field), and TM1 (nonlinear σ and ω fields) force parameters along with the phenomenological M3Y potential. See the text for details.

Wong formula [82]:

$$\sigma(E_{\rm c.m.}) = \frac{R_B^{0\,2}\hbar\omega_0}{2E_{\rm c.m.}} \ln\left[1+\exp\left(\frac{2\pi}{\hbar\omega_0}\left(E_{\rm c.m.}-V_B^0\right)\right)\right]. \tag{14}$$

This is the simple formula used in the present work to calculate the fusion cross section using the barrier characteristics such as V_B^0, R_B^0, and $\hbar\omega_0$ within the barrier penetration model for spherical nuclei. However, Wong's specific ℓ-summation procedure, leading to the use of only the $\ell = 0$ barrier, seems to exclude the modifications entering the potential due to its ℓ dependence. Therefore, a more precise formula, as given in Eq. (10), with penetrability P_ℓ given by Eqs. (12) and (13) can be employed for calculating the fusion cross section. This formula is also known as the ℓ-summed Wong formula. For details see Ref. [85]. This formula will improve the theoretical predictions as well.

III. CALCULATION AND DISCUSSION

The RMF calculations furnish the fusion hindrance reaction phenomena principally using the self-consistent relativistic mean-field formalism via the Wong formula. Parallel to the force parameter dependence of the infinite nuclear matter observables and the structural properties of finite nuclei, here one may expect the effect of force parameters on fusion characteristics. In this regard, in the first step, we calculate the M3Y potential [using Eq. (8)] and the microscopic R3Y [using Eq. (7)] *NN* potential for NL3* and TM1 force parameters. In Fig. 1, we have shown the effective *NN* interaction (in MeV) for relativistic NL-HS (linear σ, ω, and ρ fields) [70] (dotted line), NL3* (linear σ, ω, and ρ fields along with nonlinear self-interacting σ fields) [73] (dashed line), and TM1 (linear σ, ω, and ρ fields along with nonlinear self-interacting σ and ω fields) (dotted-dashed line) force parameters as a function of radius. The phenomenological M3Y potential (solid line in Fig. 1) is given for comparison. More detail of the forces and their values can be found in Refs. [18,25–27,73,75]. From the figure, one can find, that the curves from M3Y and R3Y (for NL-HS, NL3*, and TM1) interactions show similar trends. In the second step, we calculate the bulk properties such as the binding energy, the quadrupole moment Q_{20}, the total density distribution (i.e., the sum of the proton and neutron densities), the root-mean-square nuclear (neutron, proton, and charge) radii, and the single-particle energy level for nucleons. Instead of concentrating on the nuclear structure output profile for the NL3* and TM1 force parameters, we use the monopole component of the densities for the target (t) and projectile (p) as the input for estimation of the nucleus-nucleus interaction potential using Eq. (9). The expression for the spin-independent proton and neutron mean-field densities within the RMF theory is given as

$$\rho(\mathbf{R}) = \rho(r, z, \varphi). \tag{15}$$

Here r, φ, and z are the cylindrical coordinates of the radial vector $\mathbf{R}$. From the definitions given in Refs. [86,87], the nucleon density distribution functions depend on the coordinates r and z only. Explicitly, we can write the single-particle densities as

$$\rho_i(\mathbf{R}) = \rho_i(r, z) = |\Phi_i^+(r, z)|^2 + |\Phi_i^-(\mathbf{r}, z)|^2, \tag{16}$$

where $\Phi_i^\pm$ are the wave functions expanded into the eigenfunctions of an axially deformed harmonic oscillator potential in cylindrical coordinates. The normalization of the densities is given by

$$\int \rho(\mathbf{R}) d\mathbf{R} = X, \tag{17}$$

where $X = N$ and Z for the neutron number and the proton number, respectively. Further, the multipole decomposition of the density can be written in terms of even values of the multipole index λ as

$$\rho(r, z) = \sum_\lambda \rho_\lambda(\mathbf{R}) P_\lambda(\cos\theta). \tag{18}$$

The monopole component of the density distribution of the expansion in Eq. (18) is used for calculating the nucleus-nucleus optical potential. In Fig. 2, we have plotted the neutron (black solid line), proton (red solid line), and total density (green solid line) distributions for ^{58,64}Ni and ^{124,132}Sn obtained from the NL3* force and the corresponding dashed lines are for TM1 force parameter as a function of radius. In gray scale, the upper, middle and lower solid (dashed) curves in each panel are for the total (ρ_T), neutron (ρ_N), and proton (ρ_Z) densities, respectively, for the NL3* (TM1) force parameter. From the figure, one can see that the central density is a bit smaller in magnitude and is enhanced a little towards the surface region in the case of ^{124,132}Sn compared with that of ^{58,64}Ni, which is accepted to be a common feature in the heavy nucleus and plays a significant role in the scattering studies [88]. Furthermore, a very small difference in the density distributions can be found by comparing both the force parameters, which also plays a small roll in the fusion cross section in terms of nuclear interaction potential. The systematic and quantitative effects of this small relative difference of density on fusion characteristics are not analyzed in the present study.

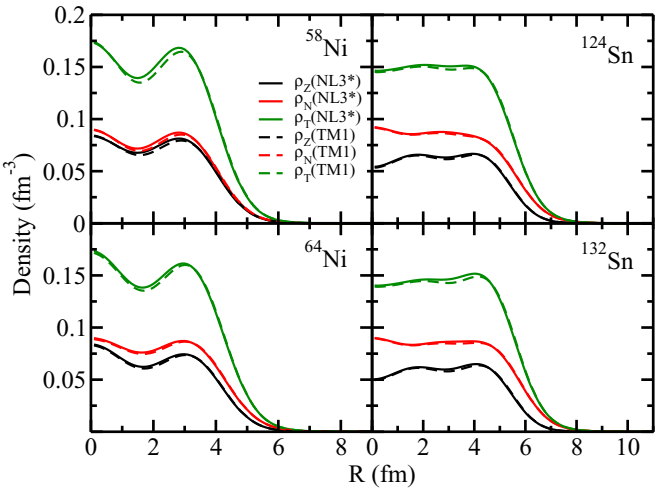

FIG. 2. The RMF (NL3* and TM1), proton (ρ_Z), neutron (ρ_N), and total (ρ_T) density distributions for ^{58,64}Ni and ^{124,132}Sn nuclei. See the text for details.

A. Nucleus-nucleus optical potential

The nuclear interaction potential $V_n(R)$ between the p and t nuclei is calculated using the well-known double-folding procedure in Eq. (9) [3,18] from respective RMF matter densities ρ_p and ρ_t for the M3Y potential and the recently developed relativistic R3Y *NN* potential. The R3Y interactions are estimated for NL3* and TM1 force parameters [19,61,62], in which the effective Lagrangian is taken to describe the nucleons' interaction through the effective mesons and electromagnetic fields. Here, we have obtained the nuclear interaction for the M3Y potential using only NL3* density. It is worth mentioning that the R3Y interaction potentials are used for the radioactivity studies of some highly unstable proton- and/or neutron-rich nuclei using the preformed cluster decay model

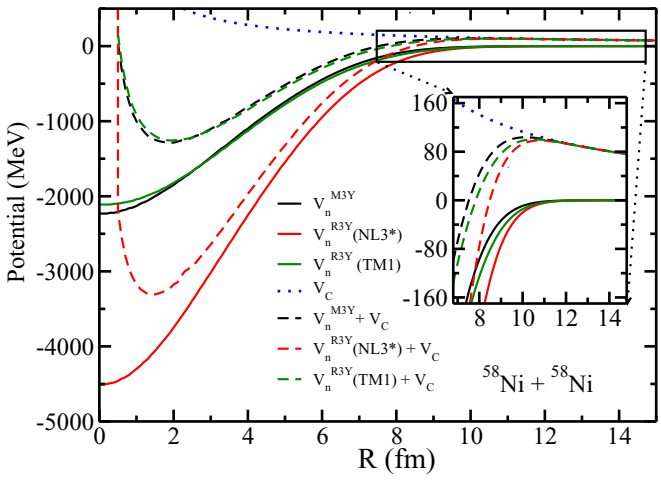

FIG. 3. The total nucleus-nucleus optical potential $V_T(R)$ and the individual contributions [the nuclear $V_n(R)$ (M3Y) and $V_n(R)$ (R3Y) for NL3* and TM1 parameter sets and the Coulomb $V_C(R)$ potential] as a function of radial separation R for ^{58}Ni + ^{58}Ni. See the text for details.

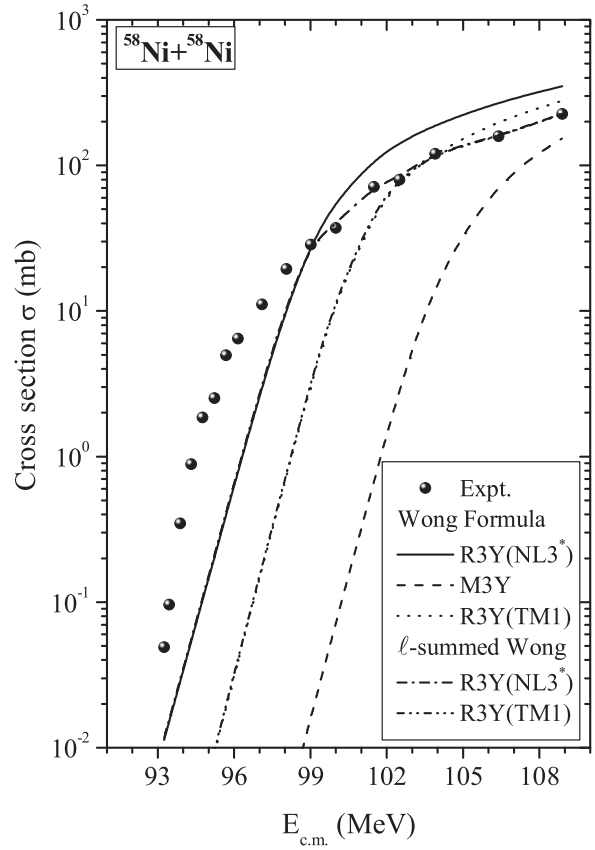

FIG. 4. Fusion-evaporation cross section as a function of center-of-mass energy $E_{c.m.}$, calculated by using the Wong formula for R3Y for NL3* (solid line), TM1 (dotted line), M3Y (dashed line) *NN* interactions along with the corresponding cross section using the ℓ-summed Wong formula and compared with experimental data for ^{58}Ni + ^{58}Ni [40]. See the text for details.

of Gupta and co-workers [18–20]. The conservation of the angular momentum in the present analysis is only limited to the ground state for the estimation of fusion characteristics of the constituent nuclei. To corelate the theoretical calculation with the experimental fusion data, one needs to adjust the spectroscopic factor by including the particle vibration coupling. Nevertheless, without this particle vibration coupling, our present formalism simply with the nonlinear σ and ω mesons in Eq. (6) is able to produce reasonable agreement with the experimental data [19]. Furthermore, these nonlinear terms in the σ and ω fields play an important role in the study of nuclear matter and the detailed nuclear structure inherited by the density while calculating the proton and cluster decay properties (mostly a surface phenomenon) [62,63,73,75].

The total interaction potentials $V_T(R) = V_n(R) + V_C(R)$ for the Ni-based reactions such as ^{58}Ni + ^{58}Ni, ^{58}Ni + ^{124}Sn, ^{58}Ni + ^{132}Sn, ^{64}Ni + ^{64}Ni, ^{64}Ni + ^{124}Sn, and ^{64}Ni + ^{132}Sn are obtained for the M3Y and R3Y interactions for NL3* densities. To examine the effect of the *NN* potential on fusion-evaporation cross sections, we have calculated the $V_n(R)$ for the ^{58}Ni + ^{58}Ni system for both NL3* and TM1 force parameters. As a representative case, the results for the nucleus-nucleus interaction potentials without the Coulomb potential for the M3Y potential (solid black line) and the

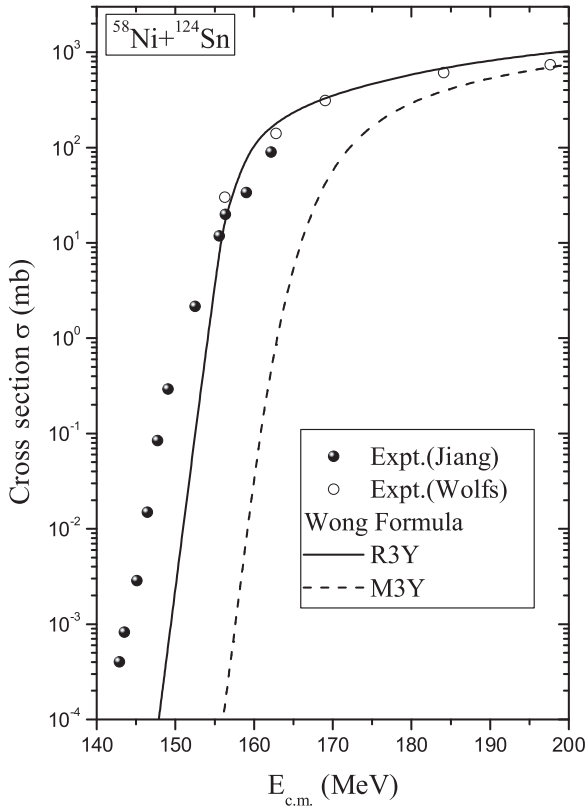

FIG. 5. Same as for Fig. 4, but for the reaction ^{58}Ni + ^{124}Sn. The experimental data are taken from Refs. [37,41,42]. See the text for details.

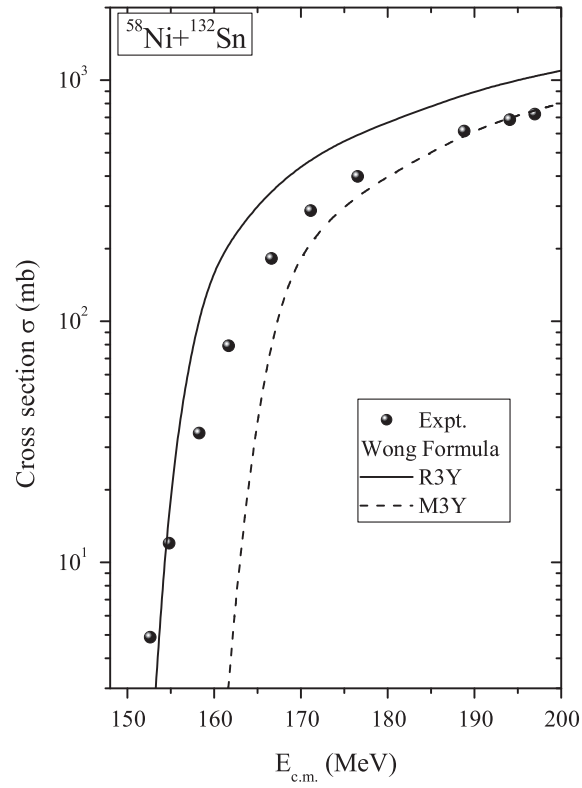

FIG. 6. Same as for Fig. 4, but for the reaction ^{58}Ni + ^{132}Sn. The experimental data are taken from Refs. [43]. See the text for details.

R3Y interactions for the NL3* (solid red line) and TM1 (solid blue line) force parameters are displayed in Fig. 3. The total interaction potentials (corresponding dashed line) along with the Coulomb potential V_C (blue dotted line) are also shown in Fig. 3. It is worth mentioning that, in gray scale, the upper, lower, and middle solid (dashed) curves are for the nuclear $V_n(R)$ potential without the Coulomb potential (with the Coulomb potential) for the relativistic TM1 and NL3* parameter sets and the phenomenological M3Y potential, respectively. From the figure, we note that the natures of the total $V_T(R)$ and the nuclear $V_n(R)$ potentials are similar for both the R3Y and M3Y *NN* interactions (see Fig. 3). Quantitatively, both the nuclear potentials obtained from M3Y and R3Y (TM1 force) differ significantly particularly in the central region from R3Y (NL3*), and this difference is reduced simultaneously with respect to the radial distance. Further, the height of the barrier for the M3Y and R3Y (TM1) *NN* interactions are a bit higher as compare to the R3Y (NL3*) case (see the inset in Fig. 3). For example, the R3Y (NL3*) case is more attractive by about 1 MeV, with a barrier height lower by a few kiloelectron volts, compared to the M3Y and R3Y (TM1) *NN* interactions, as is illustrated in the inset in Fig. 3.

B. Fusion cross sections

The barrier characteristics of the nuclear interaction potential, i.e., barrier height, position, and frequency from the total interaction potential, are used in the Wong formula [see Eq. (14)] to estimate the fusion-reaction cross sections for the systems such as ^{58}Ni + ^{58}Ni, ^{58}Ni + ^{124}Sn, ^{58}Ni + ^{132}Sn, ^{64}Ni + ^{64}Ni, ^{64}Ni + ^{124}Sn, and ^{64}Ni + ^{132}Sn, known for fusion hindrance phenomena. Figure 4 shows the comparison of the fusion cross sections obtained for ^{58}Ni + ^{58}Ni around the Coulomb barrier with the experimental data [40]. The solid line shows the fusion cross sections using the R3Y interaction and the dashed line shows the fusion cross-sections using the M3Y potential within the Wong formula for NL3* densities. In order to see the effect of the *NN* potential, the interaction potential is calculated using the double-folding procedure within the R3Y interaction for NL3* (nonlinear σ field) and TM1 (nonlinear σ and ω fields) force parameters. Figure 4 shows that the fusion cross section calculated using R3Y (TM1 force) (dotted line) lies between the R3Y (NL3* force) and M3Y interactions. It is observed using the Wong formula that the R3Y interaction with the NL3* force parameter is relatively superior to that with the TM1 force parameter and M3Y interaction in comparison with the experimental data [40] at below barrier energies. Also the M3Y interaction is a better choice at above-barrier energies within the Wong formula. However the estimate of R3Y (for both NL3* and TM1 force parameters) interactions, at energies above the barrier, is improved by adopting the ℓ-summed Wong formula [85] and this is clear from Fig. 4 as well. Further the R3Y interaction with NL3* is relatively superior to the R3Y interaction with TM1 in comparison with the experimental

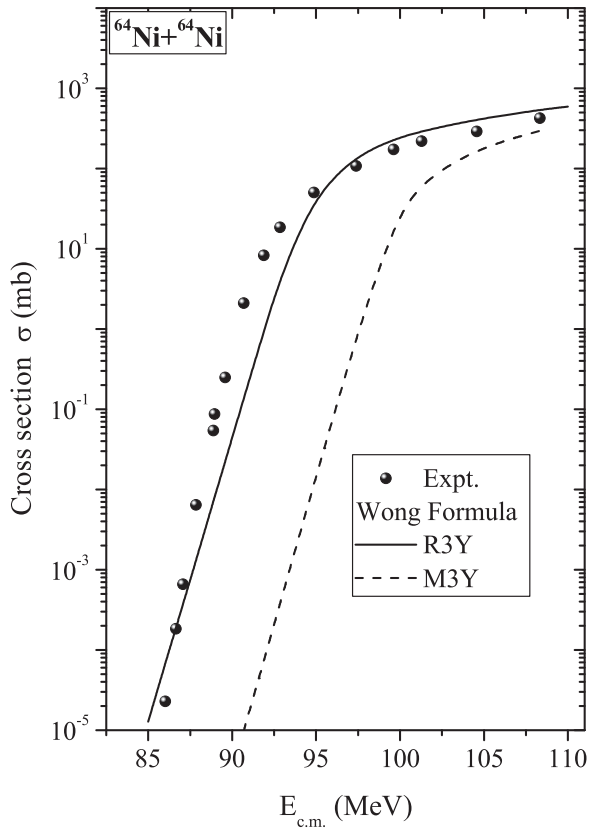

FIG. 7. Same as for Fig. 4, but for the reaction ^{64}Ni + ^{64}Ni. The experimental data are taken from Ref. [34]. See the text for details.

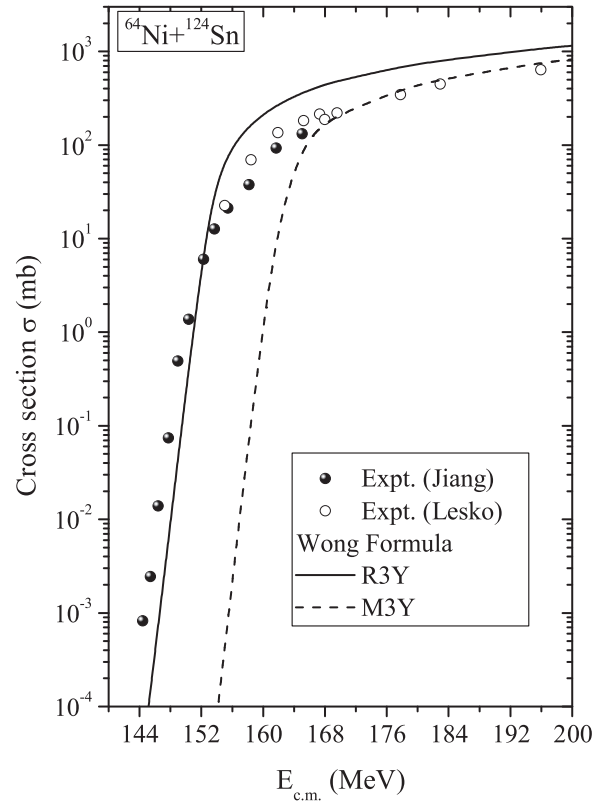

FIG. 8. Same as for Fig. 4, but for the reaction ^{64}Ni + ^{124}Sn. The experimental data are taken from Refs. [35–37]. See the text for details.

data. The ℓ_{max} values at these energies are estimated using the sharp cutoff approximation [40]. For more details one can refer to Ref. [85]. For the sake of comparison, we limit the calculations onward to the Wong formula using the R3Y interaction with NL3* and the M3Y interaction.

Motivated by these observations, the above calculations are then pursued for ^{58}Ni + ^{124}Sn and ^{58}Ni + ^{132}Sn as shown in Figs. 5 and 6, respectively. The experimental data [37,41–43] are given for comparison. For the ^{58}Ni + ^{124}Sn reaction, the experimental data [37,41,42] are available for energies near and/or below the Coulomb barrier, and for the other reaction, data are available for above the Coulomb barrier center-of-mass energies. In Figs. 5 and 6, the solid line is for the R3Y potential and the dashed line is for the M3Y potential. The cross sections corresponding to the R3Y potential are relatively close to the experimental data for energies below the Coulomb barrier, whereas the M3Y potential fits the data only at above-barrier energies. In other words, the nuclear interaction from the R3Y potential explains the cross sections at comparatively lower energies. It is to be noted that the fusion cross section corresponding to the R3Y interaction is always larger compared to that of the M3Y potential. Furthermore a few similar calculations are done for other Ni-based reactions, i.e., ^{64}Ni + ^{64}Ni, ^{64}Ni + ^{124}Sn, and ^{64}Ni + ^{132}Sn, shown in Figs. 7–9, respectively, with the experimental data [34–39]. It is clear from all these systems in Figs. 4–9 that the recently developed R3Y interaction with the NL3* force parameter has proven to be a relatively better choice than the M3Y potential for considering the fusion reactions below the barrier at low energies. In other words, the R3Y interaction allows the nuclei to relax, which reduces the barrier height and hence increases the fusion cross section.

The transmission function is used to obtain the fusion barrier distribution $\frac{d^2(E\sigma)}{dE^2}$ by differentiation with respect to center-of-mass energy. Classically, the transmission probability is a step function at an energy equal to the height of the fusion barrier. The Fermi function modifies the step function into a smoother function, a parabolic barrier. The fusion barrier distribution $\frac{d^2(E\sigma)}{dE^2}$ from fusion excitation functions are shown in Fig. 10 for the R3Y (solid line) and M3Y (dashed line) interactions. In the figure, we have shown the fusion barrier distribution for the reduced cross sections (a) ^{58}Ni + ^{58}Ni, (b) ^{58}Ni + ^{124}Sn, (c) ^{58}Ni + ^{132}Sn, (d) ^{64}Ni + ^{64}Ni, (e) ^{64}Ni + ^{124}Sn, and (f) ^{64}Ni + ^{132}Sn along with the experimental data [34–43] for comparison. As expected, here we found the similar predictions as reaction cross section, the obtained results from R3Y interaction are relatively closer to the experimental data for energies below the Coulomb barrier whereas the M3Y potential fits the data only for above-barrier energies. From the reaction cross section and the barrier distribution, one can conclude that the R3Y interaction produces relatively better results than the M3Y potential in comparison to experimental data. Hence, one can choose whole microscopic studies using the relativistic mean-field density and the recently developed

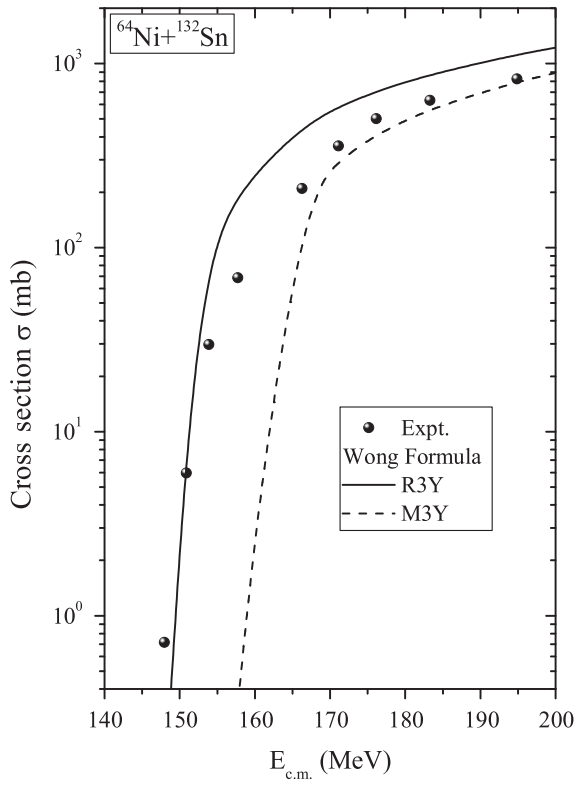

FIG. 9. Same as for Fig. 4, but for the reaction ^{64}Ni + ^{132}Sn. The experimental data are taken from Refs. [38,39]. See the text for details.

relativistic R3Y *NN* potential for fusion characteristics for the abovementioned mass region to generate the nuclear potential within the double-folding procedure.

IV. SUMMARY AND CONCLUSIONS

We have investigated possible relationships between the nucleon-nucleon interaction potential and the fusion-reaction cross section for a few Ni-based systems known for fusion hindrance phenomena. The fusion barrier distribution for the reduced fusion cross section is also estimated from fusion excitation function for R3Y and M3Y *NN* interactions. We have considered six reaction systems, namely ^{58}Ni + ^{58}Ni, ^{58}Ni + ^{124}Sn, ^{58}Ni + ^{132}Sn, ^{64}Ni + ^{64}Ni, ^{64}Ni + ^{124}Sn, and ^{64}Ni + ^{132}Sn, for the present analysis. A microscopic approach based on an axial-deformed relativistic mean-field with recently developed NL3* and TM1 forces has been used along with the Wong formula to provide a transparent and analytic way to calculate the fusion cross section by means of a convenient approach to the nucleus-nucleus optical potential. We have considered the well-known M3Y potential and the recently developed relativistic R3Y nucleon-nucleon interaction for estimating the nuclear interaction potential. The NL3* and TM1 densities for targets and projectiles are used for calculating the corresponding nuclear potential within the double-folding procedure for the study of fusion at low energies. The NL3* densities for projectiles and targets are used to obtain the nuclear interaction for the M3Y potential. It is worth mention-

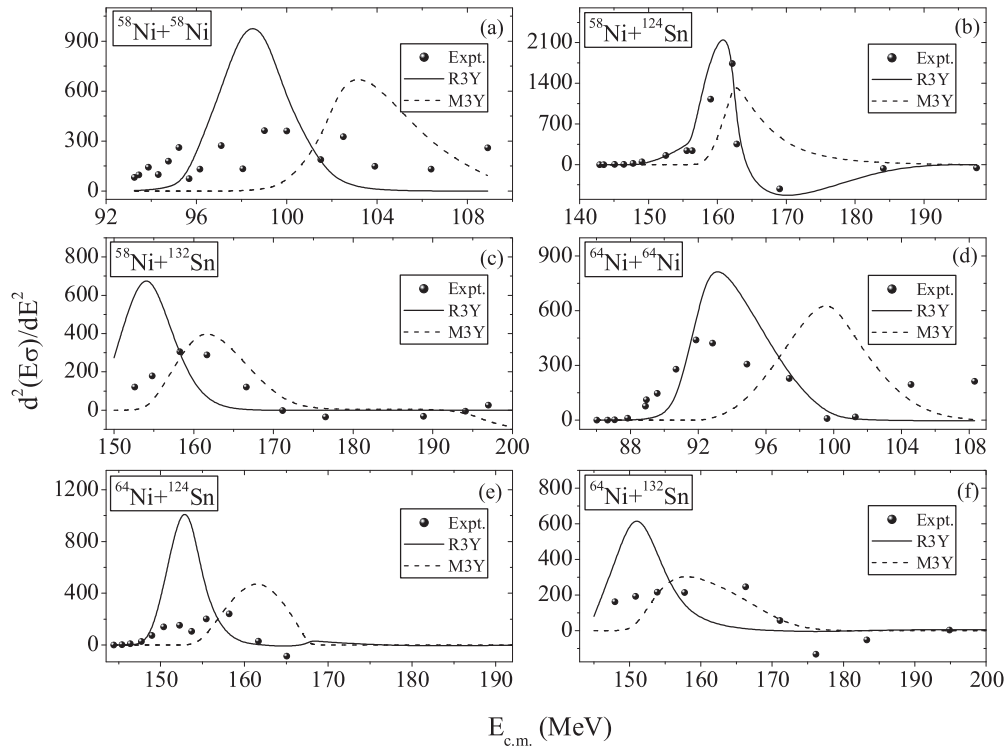

FIG. 10. The barrier distributions for the reactions (a) ^{58}Ni + ^{58}Ni, (b) ^{58}Ni + ^{124}Sn, (c) ^{58}Ni + ^{132}Sn, (d) ^{64}Ni + ^{64}Ni, (e) ^{64}Ni + ^{124}Sn, and (c) ^{64}Ni + ^{132}Sn, as a function of the center-of-mass energy. The experimental data are taken from Refs. [34–43]. See the text for details.

ing that the quadrupole, odd multipole (octupole, etc.) shape degrees of freedom, and the corresponding space reflection symmetry may provide some interesting issues and will throw more light on the fusion properties. We found that the R3Y interaction for NL3* force parameters has proven to be a better choice than the M3Y potential for considered fusion reactions below the barrier energies in the prediction of cross sections. The fusion cross sections of the R3Y interaction are improved at above-barrier energies by adopting the ℓ-summed Wong model. Further the R3Y interaction with NL3* is relatively superior to the R3Y interaction with TM1. Thus it can be inferred that the R3Y interaction with NL3* allows interacting nuclei to recline, which leads to lowering the barrier and hence increasing the cross section appreciably at the energies below the Coulomb barrier. The present analysis pursues a full microscopic study by taking the R3Y potential along with the relativistic mean-field densities within the double-folding procedure.

ACKNOWLEDGMENTS

This work has been supported by FAPESP Projects No. 2014/26195-5 and No. 2017/05660-0, INCT-FNA Project No. 464898/2014-5, the Seed Money Project of Thapar Institute of Engineering and Technology (Grant No. TU/DORSP/57/486), Department of Science and Technology (DST), Government of India Project No. YSS/2015/000342 under the Young Scientist Scheme, and the CNPq-Brasil. The authors are also thankful to the following people for various discussions and support throughout the work: B. V. Carlson, Instituto Tecnológico de Aeronáutica; R. K. Gupta, Panjab University; S. K. Patra and B. Kumar, Institute of Physics; and M. K. Sharma, Thapar Institute of Engineering and Technology.

[1] K. A. Brueckner and K. M. Watson, Phys. Rev. **92**, 1023 (1953).
[2] J. W. Alcock and W. N. Cottingham, Nucl. Phys. B **41**, 141 (1972).
[3] G. R. Satchler and W. G. Love, Phys. Rep. **55**, 183 (1979).
[4] R. V. Reid, Ann. Phys. (NY) **50**, 411 (1968).
[5] W. N. Cottingham, M. Lacombe, B. Loiseau, J. M. Richard, and R. Vinh Mau, Phys. Rev. D **8**, 800 (1973).
[6] T. Hamada and I. D. Johnston, Nucl. Phys. **34**, 382 (1962).
[7] K. E. Lassila, M. H. Hull, H. M. Ruppel, F. A. McDonald, and G. Breit, Phys. Rev. **126**, 881 (1962).
[8] B. D. Day, Phys. Rev. C **24**, 1203 (1981).
[9] V. G. J. Stoks, R. A. M. Klomp, C. P. F. Terheggen, and J. J. de Swart, Phys. Rev. C **49**, 2950 (1994).
[10] H. Yukawa, Proc. Phys. Math. Soc. Japan **17**, 48 (1935).
[11] E. Epelbaum, H.-W. Hammer, and U.-G. Meiner, Rev. Mod. Phys. **81**, 1773 (2009).
[12] F. Gross, T. D. Cohen, E. Epelbaum, and R. Machleidt, Few-Body Syst. **50**, 31 (2011).
[13] M. Garcon and J. W. Van Orden, Adv. Nucl. Phys. **26**, 293 (2001).
[14] S. Weinberg, Phys. A (Amsterdam, Neth.) **96**, 327 (1979).
[15] S. Weinberg, Phys. Lett. B **251**, 288 (1990).
[16] D. B. Kaplan, M. J. Savage, and M. B. Wise, Phys. Lett. B **424**, 390 (1998).
[17] D. B. Kaplan, M. J. Savage, and M. B. Wise, Nucl. Phys. B **534**, 329 (1998).
[18] B. B. Singh, M. Bhuyan, S. K. Patra, and R. K. Gupta, J. Phys. G: Nucl. Part. Phys. **39**, 025101 (2012).
[19] B. B. Sahu, S. K. Singh, M. Bhuyan, S. K. Biswal, and S. K. Patra, Phys. Rev. C **89**, 034614 (2014).
[20] M. Bhuyan, *Properties of Finite Nuclei Using Effective Interaction* (LAP Lambert Academic Publishing, Deutschland, Germany, 2014).
[21] U. van Kolck, Prog. Part. Nucl. Phys. **43**, 337 (1999).
[22] A. Ekström, G. Baardsen, C. Forssén, G. Hagen, M. Hjorth-Jensen, G. R. Jansen, R. Machleidt, W. Nazarewicz, T. Papenbrock, J. Sarich, and S. M. Wild, Phys. Rev. Lett. **110**, 192502 (2013).
[23] J. Boguta and A. R. Bodmer, Nucl. Phys. A **292**, 413 (1977).
[24] W. Pannert, P. Ring, and J. Boguta, Phys. Rev. Lett. **59**, 2420 (1987).
[25] S. K Singh, S. K. Biswal, M. Bhuyan, and S. K. Patra, J. Phys. G: Nucl. Part. Phys. **41**, 055201 (2014).
[26] C. Lahiri, S. K. Biswal, and S. K. Patra, Int. J. Mod. Phys. E **25**, 1650015 (2016).
[27] M. Dutra, O. Lourenço, S. S. Avancini, B. V. Carlson, A. Delfino, D. P. Menezes, C. Providência, S. Typel, and J. R. Stone, Phys. Rev. C **90**, 055203 (2014).
[28] D. A. Goldberg, S. M. Smith, H. G. Pugh, P. G. Roos, and N. S. Waal, Phys. Rev. C **7**, 1938 (1973).
[29] H. G. Bohlen, M. R. Clover, G. Ingold, H. Lettau, and W. von Oertzen, Z. Phys. A **308**, 121 (1882).
[30] E. Stiliarid, H. G. Bohlen, P. Frobrich, B. Gebauer, D. Kolbert, W. von Oertzen, M. Wilpert, and Th. Wilpert, Phys. Lett. B **223**, 291 (1989).
[31] G. L. Zhang, H. Q. Zhang, Z. H. Liu, C. L. Zhang, C. J. Lin, F. Yang, G. P. An, H. M. Jia, Z. D. Wu, X. X. Xu, C. L. Bai, and N. Yu, High Energy Phys. Nucl. Phys. **31**, 634 (2007).
[32] T. Dao Khoa and G. R. Satchler, Nucl. Phys. A **668**, 3 (2000).
[33] A. Mukherjee, M. Dasgupta, D. J. Hinde, K. Hagino, J. R. Leigh, J. C. Mein, C. R. Morton, J. O. Newton, and H. Timmers, Phys. Rev. C **66**, 034607 (2002).
[34] C. L. Jiang, K. E. Rehm, R. V. F. Janssens, H. Esbensen, I. Ahmad, B. B. Back, P. Collon, C. N. Davids, J. P. Greene, D. J. Henderson, G. Mukherjee, R. C. Pardo, M. Paul, T. O. Pennington, D. Seweryniak, S. Sinha, and Z. Zhou, Phys. Rev. Lett. **93**, 012701 (2004).
[35] K. T. Lesko, W. Henning, K. E. Rehm, G. Rosner, J. P. Schiffer, G. S. F. Stephans, B. Zeidman, and W. S Freeman, Phys. Rev. Lett. **55**, 803 (1985).
[36] K. T. Lesko, W. Henning, K. E. Rehm, G. Rosner, J. P. Schiffer, G. S. F. Stephans, B. Zeidman, and W. S. Freeman, Phys. Rev. C **34**, 2155 (1986).
[37] C. L. Jiang, A. M. Stefanini, H. Esbensen, K. E. Rehm, S. Almaraz-Calderon, M. L. Avila, B. B. Back, D. Bourgin, L. Corradi, S. Courtin, E. Fioretto, F. Galtarossa, A. Goasduff, F. Haas, M. M. Mazzocco, D. Montanari, G. Montagnoli, T. Mijatovic, R. Sagaidak, D. Santiago-Gonzalez, F. Scarlassara, E. E. Strano, and S. Szilner, Phys. Rev. C **91**, 044602 (2015).

[38] J. F. Liang, D. Shapira, J. R. Beene, C. J. Gross, R. L. Varner, A. Galindo-Uribarri, J. Gomez del Campo, P. A. Hausladen, P. E. Mueller, D. W. Stracener, H. Amro, J. J. Kolata, J. D. Bierman, A. L. Caraley, K. L. Jones, Y. Larochelle, W. Loveland, and D. Peterson, Phys. Rev. C **75**, 054607 (2007).
[39] J. F. Liang, D. Shapira, C. J. Gross, R. L. Varner, J. R. Beene, P. E. Mueller, and D. W. Stracener, Phys. Rev. C **78**, 047601 (2008).
[40] M. Beckerman, J. Ball, H. Enge, M. Salomaa, A. Sperduto, S. Gazes, A. DiRienzo, and J. D. Molitoris, Phys. Rev. C **23**, 1581 (1981).
[41] F. L. H. Wolfs, W. Henning, K. E. Rehm, and J. P. Schiffer, Phys. Lett. B **196**, 113 (1987).
[42] F. L. H. Wolfs, Phys. Rev. C **36**, 1379 (1987).
[43] Z. Kohley, J. F. Liang, D. Shapira, R. L. Varner, C. J. Gross, J. M. Allmond, A. L. Caraley, E. A. Coello, F. Favela, K. Lagergren, and P. E. Mueller, Phys. Rev. Lett. **107**, 202701 (2011).
[44] R. Vandenbosch, Annu. Rev. Nucl. Part. Sci. **42**, 447 (1992).
[45] A. B. Balantekin and N. Takigawa, Rev. Mod. Phys. **70**, 77 (1998).
[46] N. Rowley, G. R. Satchler, and P. H. Stelson, Phys. Lett. B **254**, 25 (1991).
[47] C. Vaz *et al.*, Phys. Rep. **69**, 373 (1981).
[48] R. G. Stokstad, Y. Eisen, S. Kaplanis, D. Pelte, U. Smilansky, and I. Tserruya, Phys. Rev. Lett. **41**, 465 (1978).
[49] R. G. Stokstad, Y. Eisen, S. Kaplanis, D. Pelte, U. Smilansky, and I. Tserruya, Phys. Rev. C **21**, 2427 (1980).
[50] C. L. Jiang, H. Esbensen, K. E. Rehm, B. B. Back, R. V. F. Janssens, J. A. Caggiano, P. Collon, J. Greene, A. M. Heinz, D. J. Henderson, I. Nishinaka, T. O. Pennington, and D. Seweryniak, Phys. Rev. Lett. **89**, 052701 (2002).
[51] C. J. Lin, Phys. Rev. Lett. **91**, 229201 (2003).
[52] C. L. Jiang, B. B. Back, H. Esbensen, R. V. F. Janssens, and K. E. Rehm, Phys. Rev. C **73**, 014613 (2006).
[53] C. L. Jiang, B. B. Back, R. V. F. Janssens, and K. E. Rehm, Phys. Rev. C **75**, 057604 (2007).
[54] K. Hagino, N. Rowley, and M. Dasgupta, Phys. Rev. C **67**, 054603 (2003).
[55] C. L. Jiang, K. E. Rehm, B. B. Back, H. Esbensen, R. V. F. Janssens, A. M. Stefanini, and G. Montagnoli, Phys. Rev. C **89**, 051603(R) (2014).
[56] M. Dasgupta and D. J. Hinde, Annu. Rev. Nucl. Part. Sci. **48**, 401 (1998).
[57] B. D. Serot and J. D. Walecka, in *Advances in Nuclear Physics*, edited by J. W. Negele and Erich Vogt (Plenum Press, New York, 1986), Vol. 16, p. 1.
[58] S. K. Singh, M. Bhuyan, P. K. Panda, and S. K. Patra, J. Phys. G: Nucl. Part. Phys. **40**, 085104 (2013).
[59] S. K. Patra, M. Bhuyan, M. S. Mehta, and R. K. Gupta, Phys. Rev. C **80**, 034312 (2009).
[60] M. Bhuyan, S. K. Patra, and R. K. Gupta, Phys. Rev. C **84**, 014317 (2011).
[61] M. Bhuyan, Phys. Rev. C **92**, 034323 (2015).
[62] M. Bhuyan, B. V. Carlson, S. K. Patra, and S.-G. Zhou, Phys. Rev. C **97**, 024322 (2018).
[63] M. Bhuyan, Phys. At. Nucl. **81**, 15 (2018).
[64] G. A. Lalazissis, S. Raman, and P. Ring, At. Data Nucl. Data Tables **71**, 1 (1999).
[65] P.-G. Reinhard, Rep. Prog. Phys. **52**, 439 (1989).
[66] P. Ring, Prog. Part. Nucl. Phys. **37**, 193 (1996).
[67] D. Vretenar, A. V. Afanasjev, G. A. Lalazissis, and P. Ring, Phys. Rep. **409**, 101 (2005).
[68] J. Meng, H. Toki, S. G. Zhou, S. Q. Zhang, W. H. Long, and L. S. Geng, Prog. Part. Nucl. Phys. **57**, 470 (2006).
[69] N. Paar, D. Vretenar, and G. Colo, Rep. Prog. Phys. **70**, 691 (2007).
[70] C. J. Horowitz and B. D. Serot, Nucl. Phys. A **368**, 503 (1981).
[71] T. Niksić, D. Vretenar, and P. Ring, Prog. Part. Nucl. Phys. **66**, 519 (2011).
[72] X.-F. Zhao, and H.-Y. Jia, Phys. Rev. C **85**, 065806 (2012).
[73] G. A. Lalazissis, S. Karatzikos, R. Fossion, D. Pena Arteaga, A. V. Afanasjev, and P. Ring, Phys. Lett. B **671**, 36 (2009).
[74] M. Bender, P.-H. Heenen, and P.-G. Reinhard, Rev. Mod. Phys. **75**, 121 (2003).
[75] Y. Sugahara and H. Toki, Nucl. Phys. A **579**, 557 (1994).
[76] L. I. Schiff, Phys. Rev. **84**, 1 (1951).
[77] D. Vautherin and M. Veneroni, Phys. Lett. B **29**, 203 (1969).
[78] S. Karatzikos, A. V. Afanasjev, G. A. Lalazissis, and P. Ring, Phys. Lett. B **689**, 72 (2010).
[79] J. Dobaczewski, H. Flocard, and J. Treiner, Nucl. Phys. A **422**, 103 (1984).
[80] D. G. Madland and J. R. Nix, Nucl. Phys. A **476**, 1 (1981).
[81] P. Möller and J. R. Nix, At. Data Nucl. Data Tables **39**, 213 (1988).
[82] C. Y. Wong, Phys. Rev. Lett. **31**, 766 (1973).
[83] D. L. Hill and J. A. Wheeler, Phys. Rev. **89**, 1102 (1953).
[84] T. D. Thomas, Phys. Rev. **116**, 703 (1959).
[85] R. Kumar, M. Bansal, S. K. Arun, and R. K. Gupta, Phys. Rev. C **80**, 034618 (2009).
[86] D. Vautherin and D. M. Brink, Phys. Rev. C **5**, 626 (1972).
[87] E. Moya de Guerra, P. Sarriguren, J. A. Caballero, M. Casas, and D. W. L. Sprung, Nucl. Phys. A **529**, 68 (1991).
[88] M. Bhuyan, R. N. Panda, T. R. Routray, and S. K. Patra, Phys. Rev. C **82**, 064602 (2010).